

REAL-TIME TOTAL FOCUSING METHOD IMAGING FOR ULTRASONIC INSPECTION OF THREE-DIMENSIONAL MULTILAYERED MEDIA

Wenkai Cui, Kaihuai Qin*

Department of Computer Science and Technology, Tsinghua University, Beijing, China

ABSTRACT

In non-destructive testing of three-dimensional media, the total focusing method (TFM) draws attentions of numerous researchers owing to its ability to provide image with superior quality. But its application in multilayered media is limited by the computation complexity of calculating point of incidence (POI) and increased quantity of acquired ultrasonic data. This paper presents a novel 3D-TFM called linear scan-conversion (LSC) 3D-TFM for the imaging of 3D multilayered media, which uses the scan-conversion algorithm of line segment to substitute traditional ray-tracing method to calculate POI. The iterative computations in ray-tracing method can be avoided, which reduces the time complexity by one order of magnitude. The simulation experiment indicates that LSC 3D-TFM speeds up the imaging process 28 times while maintaining the same result.

Index Terms—Ultrasonic phased array, Multi-layered object, Total focusing method, Full matrix capture

1. INTRODUCTION

In non-destructive testing (NDT), ultrasonic phased-array systems are becoming more and more attractive to researchers due to their flexibility and simplicity. An advanced data acquisition technique full matrix capture (FMC) and its post-processing algorithm total focusing method (TFM) [1] are frequently used in industrial inspection [2] [3] [4] [5] because of its benefits in defect characterization and image resolution.

In the inspection process, a phased array need to be coupled with the tested object, which is proved to be problematic if its surface is non-planar. One way to overcome this problem is using a phased-array where every phased-array element is flexible to tightly contact the tested object [6] [7] [8], but manufacture such a flexible phased array is more complicated and costly. The most common used solution is coupling the tested object via an intermediary medium such as water, which is referred as immersion testing.

In the imaging of multilayered object such as immersion testing, the sound wave is refracted when it reaches the interface between different media. To acquire the accurate

sound propagation path, the Snell's law and Fermat's principle are introduced to calculate the point of incidence (POI) [9] [10] [11]. TFM is combined with ray-tracing method [12] [13] to acquire an accurate image of multilayered object's structure. But both the iterative calculation of POI and TFM require high computational power, especially for three-dimensional object, which restricts its practical application. There has been multiple methods to improve the performance of TFM. Using GPU hardware to accelerate the imaging process is proved to be the most effective way owing to its high parallelizability [14] [15] [16], but it needs appropriate platform and additional programming. Although reducing the number of phased array element without changing the effective aperture can also speed up the imaging process, other problems such as side lobes may affect the precision of the result image [17]. By extending the phased shift migration (PSM), the frequency-domain TFM [18] [19] [20] is proposed to eliminate the time-consuming calculation of POI, which brings a tremendous improvement compared to time-domain TFM, but it can't deal with objects with irregular interface profile.

Based on the scan-conversion algorithm of line segment in computer graphics, the motion trajectory method is capable of acquiring multiple incident points simultaneously [16]. This paper extends this algorithm to the three-dimensional multilayered object, which makes real-time 3D imaging possible. 3D ultrasonic data can be acquired by 2D phased array or using 1D array to sweep across the tested object [21] [22]. This paper focuses on 2D phased array to acquire ultrasonic data.

2. ALGORITHM THEORY

2.1. Total focusing method combined with ray-tracing

Based on delay-and-sum principle, total focusing method (TFM) is able to achieve focus at every point. The pixel value of $p(x, y, z)$ in the result image is expressed as follows:

$$I[p(x, y, z)] = \sum_{t=0}^{N-1} \sum_{r=0}^{N-1} S_{t,r}(T_t(x, y, z) + T_r(x, y, z)) \quad (1)$$

Where N is the number of elements in the phased array, the subscripts t and r denote the indices of transmitter and receiver respectively, $S_{t,r}$ represents the received signal corresponding to the transmitter-receiver pair (E_t, E_r) and

* Corresponding author

$T_t(x, y, z)$ (or $T_r(x, y, z)$) is the ultrasound transmission time from E_t (or E_r) to $p(x, y, z)$.

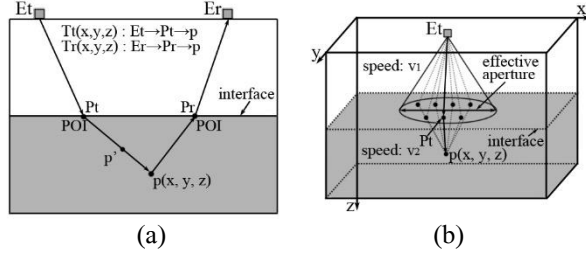


Fig. 1. Total focusing method combined with ray-tracing. (a) Sound propagation path in multilayered object. Every pixel p' on refractive vector shares the same incident point P_t . (b) Iterative method to calculate POI in 3D tested object.

For imaging of multilayered object, the sound propagation path in Fig. 1(a) is refracted because of sound speed variation in the different layers. To acquire accurate propagation path, the point of incidence (POI) need to be located. There exists three main algorithms to calculate POI: the iterative, analytical and numerical methods [10]. The iterative method is suitable for both planar and non-planar interface, which becomes the most common used method: as is shown in Fig. 1(b), for every point P_t on the interface within the element's effective aperture, calculate the transmission time along the propagation path $E_t \rightarrow P_t \rightarrow p$: $\frac{|E_t P_t|}{v_1} + \frac{|P_t p|}{v_2}$. According to Fermat's Law, the point of incidence is the one with the minimum transmission time.

2.2. 3D motion trajectory method

As is shown in Fig. 1(a), every point on the identical propagation path shares the same POI [16]: $\vec{E_t P_t}$ and $\vec{P_t p}$ are the incident vector and refractive vector respectively, where P_t represents the incident point. For every point p' on line $P_t p$, the corresponding POI between E_t and p is also P_t .

For every point P_t on the interface within E_t 's effective aperture, when the beam emitted by element E_t arrives at point P_t , we calculate the refraction vector based on the Snell's law, then adapt the line scan-conversion algorithm in computer graphics to acquire the coordinate of point on the refraction vector $\vec{P_t p}$. Therefore, for every point p' on $\vec{P_t p}$, its transmission time is $T_t(p') = \frac{|E_t P_t|}{v_1} + \frac{|P_t p'|}{v_2}$.

Based on the identical principle, motion trajectory method is extended into the ultrasonic imaging of 3D multilayered object. First, all points within the element's sound field is divided into multiple regions. Then for each region, linearly interpolate line segments to pass through every point in this region.

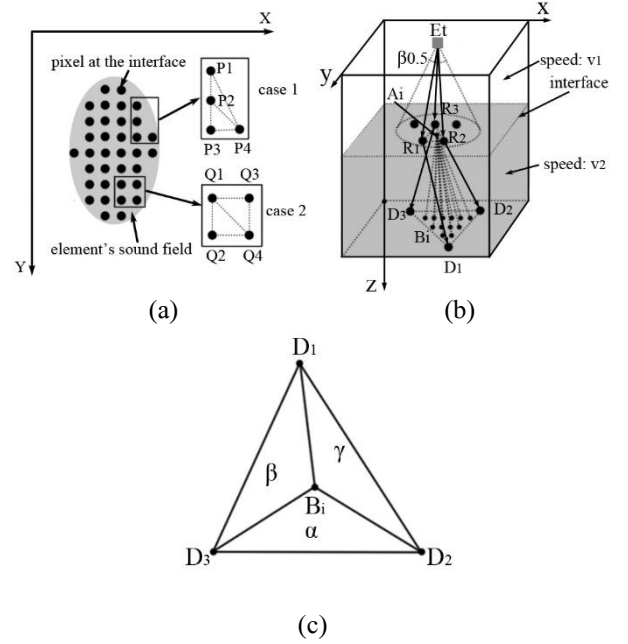


Fig. 2. 3D motion trajectory method. (a) Divide pixels on the interface into tuples. Each tuple contains three adjacent points. (b) Every tuple corresponds to a region bounded by the refraction vector. Linearly interpolate line segments to cover all points in this region. (c) Three parameters α, β, γ to locate A_i in triangle $\Delta R_1 R_2 R_3$.

Fig. 2(a) and Fig. 2(b) describe how to divide element's sound field into multiple regions. All points on the interface within the element's sound field are divided into multiple tuples where each tuple contains three adjacent incident points. Fig. 2(a) shows two different cases in dividing adjacent points into tuples. In case 1, four adjacent points P_1, P_2, P_3, P_4 are divided into two result tuples $(P_1, P_2, P_4), (P_2, P_3, P_4)$. In case 2, the result tuples are $(Q_1, Q_3, Q_4), (Q_1, Q_2, Q_4)$.

For each tuple, calculate the refractive vectors of three points in this tuple. (R_1, R_2, R_3) represents three incident points on the interface in one tuple, $\vec{R_1 D_1}, \vec{R_2 D_2}, \vec{R_3 D_3}$ are their refractive vectors and D_1, D_2, D_3 are on the lower boundary of the tested object. Therefore, the region corresponding to (R_1, R_2, R_3) is bounded by line segments $R_1 D_1, R_2 D_2, R_3 D_3$. However, every point $p(x, y, z)$ within the region bounded by line segments $R_1 D_1, R_2 D_2, R_3 D_3$ is not passed by refraction vectors, whose transmission time $T_t(x, y, z)$ is still unknown. To calculate the transmission time of every point in the region, multiple lines are linearly interpolated between three refraction vectors.

For every pixel B_i within the triangle $\Delta D_1 D_2 D_3$ in Fig. 2(c), the position of $B_i = \alpha D_1 + \beta D_2 + \gamma D_3$ can be described using three parameters α, β, γ :

$$\alpha = \frac{S_{\Delta B_i D_2 D_3}}{S_{\Delta D_1 D_2 D_3}}, \beta = \frac{S_{\Delta D_1 B_i D_3}}{S_{\Delta D_1 D_2 D_3}}, \gamma = \frac{S_{\Delta D_1 D_2 B_i}}{S_{\Delta D_1 D_2 D_3}} \quad (2)$$

Where $S_{\Delta D_1 D_2 D_3}$ is the square of the triangle $\Delta D_1 D_2 D_3$ and $\alpha + \beta + \gamma = 1$. B_i 's corresponding point A_i in triangle $\Delta R_1 R_2 R_3$ is expressed as follows:

$$A_i = \alpha R_1 + \beta R_2 + \gamma R_3 \quad (3)$$

Hence, $\overrightarrow{EA_i}$ and $\overrightarrow{A_i B_i}$ are the incident vector and the refraction vector, respectively. Then the line scan-conversion algorithm is adapted to get every point on the refraction vector $\overrightarrow{A_i B_i}$, the transmission time of every point in this region is acquired.

The entire 3D motion trajectory method to calculate the transmission time $T_t(x, y, z)$ of every point in result image for element E_t is described as follows:

Algorithm 1 3D motion trajectory method

Input: $E_t(x_t, y_t, 0)$, interface: $B(x, y, z) = 0$.

Output: $T_t(x, y, z), 0 \leq x < X_L, 0 \leq y < Y_L, 0 \leq z < Z_L$.

1. Acquire all points on the interface within element's sound field, then divide the acquired points into tuples (Fig. 2(a)). For every tuple (R_1, R_2, R_3) , perform 2-3.
 2. Calculate the refraction vectors $\overrightarrow{R_1 D_1}, \overrightarrow{R_2 D_2}, \overrightarrow{R_3 D_3}$ based on the Snell's Law and linearly interpolate line segments $A_i B_i$ among the refraction vectors. For every line segment $A_i B_i$, perform 3.
 3. Adapt the line scan-conversion algorithm to get every point p' on the line $A_i B_i$. The transmission time of p' is $T_t(p') = \frac{|E_t A_i|}{v_1} + \frac{|A_i p'|}{v_2}$.
-

2.3. LSC 3D-TFM

Based on the 3D motion trajectory method, the entire LSC 3D-TFM algorithm for the imaging of 3D multilayered object is shown in Algorithm 2.

Algorithm 2 LSC 3D-TFM

Input: the full matrix $S_{t,r}, E_k(x_k, y_k, 0), 0 \leq t, r, k < N$.

Output: $I(x, y, z), 0 \leq x < X_L, 0 \leq y < Y_L, 0 \leq z < Z_L$.

1. By assuming the tested object is homogeneous, the imaging algorithm for homogeneous 3D object is adapted to get the interface $B(x, y, z) = 0$ between two different layers.
 2. For every element $E_k, 0 \leq k < N$ in the phased array, adapt 3D motion trajectory method to calculate the transmission time $T_k(x, y, z)$ for every point $p(x, y, z)$ in the image.
 3. Use (1) to get the value of every point in the result image.
-

In traditional TFM with ray-tracing, the time complexity of the iterative method is $O(X_L \cdot Y_L)$ and the total time complexity to calculate the transmission time $T_t(x, y, z)$ for every element-pixel pair $(E_t, p(x, y, z)), 0 \leq t < N$ is $O(N \cdot X_L^2 \cdot Y_L^2 \cdot Z_L)$. While in 3D motion trajectory method, the line scan-conversion algorithm with time complexity $O(Z_L)$ is called $O(X_L \cdot Y_L)$ times. Therefore, the time complexity of step 2 in Algorithm 2 is $O(N \cdot X_L \cdot Y_L \cdot Z_L)$ which improves the imaging procedure by two orders of magnitude. Besides,

the iterative method involves lots of root-mean-square computations in calculating the transmission time and most calculations in LSC-TFM is addition and multiplication, which indicates an even better performance improvement.

3. EXPERIMENT

The immersion testing experiment is simulated by k-wave [23] software package in Matlab to get the full matrix. The structure of tested object is shown in Fig. 3. The number of elements in 2D phased array is $4 \times 9 = 36$. The size of the tested object is $2.5\text{mm} \times 5\text{mm} \times 5\text{mm}$ and the depth of the interface between different media is 2.25mm . There are three holes of diameter 0.1mm inside to simulate the defects of the object. The coordinates of three holes are $(0.25\text{mm}, 1\text{mm}, 3.25\text{mm})$, $(0.75\text{mm}, 2\text{mm}, 3.75\text{mm})$ and $(1.25\text{mm}, 3\text{mm}, 4.25\text{mm})$.

The preprocessing 3D-TFM combined with ray-tracing and LSC 3D-TFM are used to process the full matrix acquired through simulation. All algorithms are running on a PC with Intel® Core™ i5-4210 CPU @ 1.7GHz and 4GB RAM and their result images are displayed in Fig. 4 (x-y plane) and Fig. 5 (y-z plane), respectively. The range of pixel value in result images is $[0, 255]$.

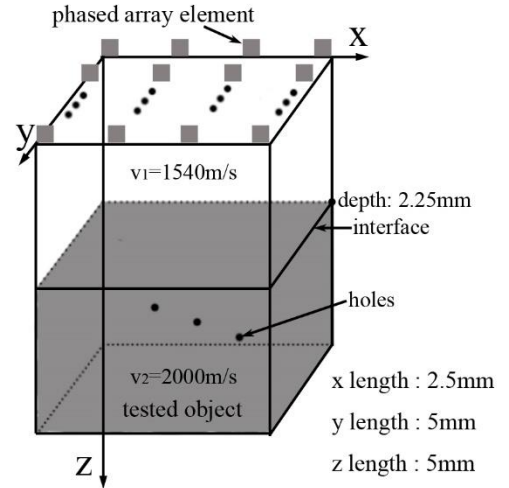


Fig. 3. Structure of tested object. Three spherical holes inside the tested object.

To easily compare the result images, the result image of the traditional TFM combined with ray-tracing (Fig. 4(a), Fig. 5(a)) are selected as the reference. The difference images between the traditional TFM and LSC 3D-TFM (Fig. 4(b), Fig. 5(b)) are shown in Fig. 4(c) and Fig. 5(c). According to Fig. 4(c) and Fig. 5(c), the maximum difference is only 6 and the average absolute value of the difference image between both algorithms is 0.2685. The slight difference between both algorithms is caused by the line scan-conversion algorithm in 3D motion trajectory method. As is shown in Fig. 6, to calculate the transmission time $T_t(p)$ from element E_t to pixel p , the propagation path in traditional TFM is $E_t \rightarrow P_i \rightarrow p$ and the transmission time is $T_t(p) = \frac{|E_t P_i|}{v_1} + \frac{|P_i p|}{v_2}$. In LSC-

TFM, the actual propagation path is $E_t \rightarrow P_i' \rightarrow p'$ and the corresponding time is $T_t'(p) = \frac{|E_t P_i'|}{v_1} + \frac{|P_i' p'|}{v_2}$. Suppose the pixel pitch in result image is I_a , we can get $|P_i P_i'| < \frac{I_a}{2}$, $|pp'| < \frac{I_a}{2}$. As $v_1 < v_2$,

$$|T_t(p) - T_t'(p)| < \left| \frac{|P_i P_i'|}{v_1} + \frac{|pp'|}{v_2} \right| < \frac{I_a}{v_1}$$

Therefore, the average absolute value of the difference image between both algorithms decreases as I_a decrease, which can also be drawn from Table 1.

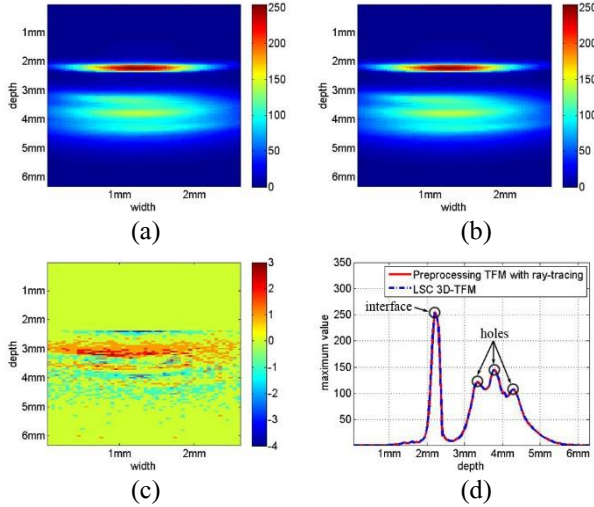


Fig. 4. Result images at x-z plane constructed by (a) Preprocessing TFM with ray-tracing, processing time: 2702.2s. (b) LSC 3D-TFM, processing time: 95.997s. (c) Difference image between (a) and (b). (d) Maximum amplitudes along the depth direction. Four peaks correspond to the interface and three holes.

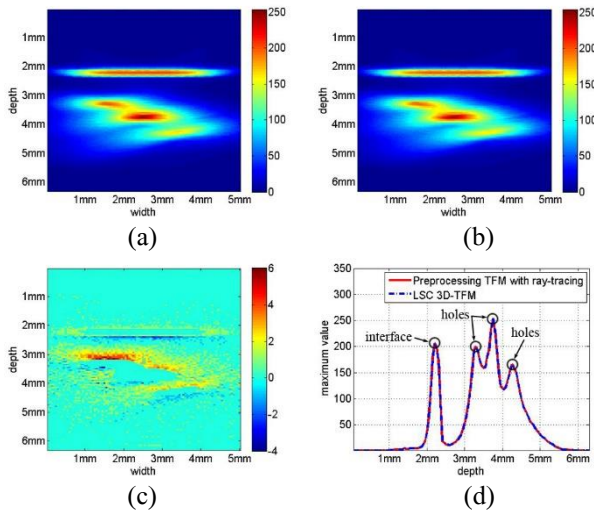


Fig. 5. Result images at y-z plane constructed by (a) Preprocessing TFM with ray-tracing. (b) LSC 3D-TFM. (c) Difference image between (a) and (b). (d) Maximum amplitudes along the depth direction.

The maximum amplitudes along the depth direction are plotted in Fig. 4(d) (Fig. 5(d)). Every plot contains four peaks and both plots coincide with each other. The first peak indicates the interface between different media and the last three peaks corresponds to three holes in tested object, respectively. Thus, there are no difference in locating the defects in tested object between both algorithms, which verifies the correctness of LSC 3D-TFM. But the running time of LSC 3D-TFM (95.997s) is 28 times faster than the conventional algorithm (2702.2s).

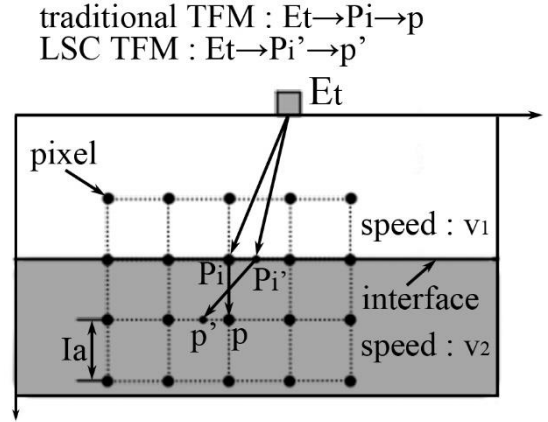


Fig. 6. The difference between traditional TFM with ray-tracing and LSC-TFM in calculating the transmission time $T_t(p)$. In LSC-TFM, P_i' is acquired from interpolation between adjacent pixels on the interface and p' is obtained from line scan-conversion algorithm.

Table 1. The average difference between traditional TFM and LSC-TFM under different pixel pitch (I_a).

Pixel Pitch I_a (mm)	0.1	0.0625	0.05
Average Difference	0.7553	0.5485	0.2685

4. CONCLUSION

In the imaging of multilayered objects, the iterative method to calculate POI is adapted to acquire the accurate propagation path, which greatly increase its time complexity. This paper proposes a novel TFM algorithm LSC 3D-TFM which brings a great performance improvement. Combined with the line scan-conversion algorithm, the 3D motion trajectory method is able to get multiple incident points at the same time, which not only reduces the time complexity of the imaging algorithm, but also uses addition and multiplication to substitute the time-consuming root mean square calculation. The simulation experiment proves the correctness and effectiveness of LSC 3D-TFM by comparing its result image and running time to that of the traditional TFM with ray-tracing. Besides, further performance improvement can be achieved by combing LSC 3D-TFM with other existing optimization methods such as GPU.

5. REFERENCES

- [1] C. Holmes, B.W. Drinkwater, and P.D. Wilcox, "Post-processing of the full matrix of ultrasonic transmit-receive array data for non-destructive evaluation," *NDT & E International*, vol. 38, no. 8, pp. 701-711, 2005.
- [2] R.T. Grotenhuis, A. Hong, and A. Sakuta, "Inspection of complex geometries using the full matrix capture (FMC) method," *9th Int Conf on NDE in Relation to Structural Integrity for Nuclear and Pressurized Components*, Seattle WA, USA, 2012.
- [3] A. Aschy, N. Terrien, S. Robert, and M. Bentahar, "Enhancement of the total focusing method imaging for immersion testing of anisotropic carbon fiber composite structures," *AIP Conference Proceedings*, vol. 1806, no. 1, pp. 040005, 2017.
- [4] N. Quaegebeur, and P. Masson, "Correlation-based imaging technique using ultrasonic transmit-receive array for Non-Destructive Evaluation," *Ultrasonics*, vol. 52, no. 8, pp. 1056-1064, 2012.
- [5] O. Oralkan, A.S. Ergun, J.A. Johnson, M. Karaman, U. Demirci, K. Kaviani, T.H. Lee, and B.T. Khuri-Yakub, "Capacitive micromachined ultrasonic transducers: Next-generation arrays for acoustic imaging?," *Ultrasonics, Ferroelectrics, and Frequency Control, IEEE Transactions on*, vol. 49, no. 1, pp. 1596-1610, 2002.
- [6] J.W. Mackersie, G. Harvey, and A. Gachagan, "DEVELOPMENT OF AN EFFICIENT CONFORMABLE ARRAY STRUCTURE," *AIP Conference Proceedings*, vol. 1096, no. 1, pp. 785-791, 2009.
- [7] K. Shi, K. Que, and D. Guo, "Flexible ultrasonic phased-array probe," *Tsinghua Science and Technology*, vol. 9, no. 5, pp. 574-577, 2004.
- [8] A.J. Hunter, B.W. Drinkwater, and P.D. Wilcox, "Autofocusing ultrasonic imagery for non-destructive testing and evaluation of specimens with complicated geometries," *NDT & E International*, vol. 43, no. 2, pp. 78-85, 2010.
- [9] M. Weston, P. Mudge, C. Davis, and A. Peyton, "Time efficient auto-focussing algorithms for ultrasonic inspection of dual-layered media using Full Matrix Capture," *NDT & E International*, vol. 47, pp. 43-50, 2012.
- [10] M. Weston, "Advanced Ultrasonic Digital Imaging and Signal Processing for Applications in the Field of Non-Destructive Testing," 2012.
- [11] M. Sutcliffe, M. Weston, P. Charlton, and I. Cooper, "Full matrix capture with time-efficient auto-focusing of unknown geometry through dual-layered media," *Insight-Non-Destructive Testing and Condition Monitoring*, vol. 55, no. 6, pp. 297-301, 2013.
- [12] J.A. Ogilvy, "An iterative ray tracing model for ultrasonic nondestructive testing," *NDT & E International*, vol. 25, no. 1 pp. 3-10, 1992.
- [13] A. Shlivinski, and K.J. Langenberg, "Defect imaging with elastic waves in inhomogeneous-anisotropic materials with composite geometries," *Ultrasonics*, vol. 46, no. 1, pp. 89-104, 2007.
- [14] M. Sutcliffe, M. Weston, B. Dutton, P. Charlton, and K. Donne, "Real-time full matrix capture for ultrasonic non-destructive testing with acceleration of post-processing through graphic hardware," *NDT & E International*, vol. 51, pp. 16-23, 2012.
- [15] D. Romero-Laorden, J. Villazon-Terrazas, O. Martinez-graullera, A. Ibanez, M. Parrilla, and M.S. Penas, "Analysis of parallel computing strategies to accelerate ultrasound imaging processes," *IEEE Transactions on Parallel and Distributed Systems*, vol. 27, no. 12, pp. 3429-3440, 2016.
- [16] C. Yang, K. Qin, and Y. Li, "Real-time ultrasonic imaging for multi-layered objects with synthetic aperture focusing technique," *Instrumentation and Measurement Technology Conference (I2MTC) Proceedings, 2014 IEEE International*, pp. 561-566, 2014.
- [17] S.C. Wooh, and Y. Shi, "Influence of phased array element size on beam steering behavior," *Ultrasonics*, vol. 36, no. 6, pp. 737-749, 1998.
- [18] H. Wu, J. Chen, K. Yang, and X. Hu, "Ultrasonic array imaging of multilayer structures using full matrix capture and extended phase shift migration," *Measurement Science and Technology*, vol. 27, no. 4, pp. 045401, 2016.
- [19] A.J. Hunter, B.W. Drinkwater, and P.D. Wilcox, "The wavenumber algorithm for full-matrix imaging using an ultrasonic array," *Ultrasonics, Ferroelectrics, and Frequency Control, IEEE Transactions on*, vol. 55, no. 11, pp. 2450-2462, 2008.
- [20] M.H. Skjelvareid, T. Olofsson, and Y. Birkelund, "Three-dimensional ultrasonic imaging in multilayered media," *AIP Conference Proceedings*, vol. 1433, no. 1, pp. 169-172, 2012.
- [21] R.W. Prager, U.Z. Ijaz, A.H. Gee, and G.M. Treece, "Three-dimensional ultrasound imaging," *Proceedings of the Institution of Mechanical Engineers, Part H: Journal of Engineering in Medicine*, vol. 224, no. 2, pp. 193-223, 2010.
- [22] C. Holmes, B.W. Drinkwater, and P.D. Wilcox, "Advanced post-processing for scanned ultrasonic arrays: Application to defect detection and classification in non-destructive evaluation," *Ultrasonics*, vol. 48, no. 6, pp. 636-642, 2008.
- [23] B.E. Treeby, and B.T. Cox, "k-Wave: MATLAB toolbox for the simulation and reconstruction of photoacoustic wave-fields," *Journal of Biomedical Optics*, vol. 15, no. 2, pp. 021314, 2010.